Development and validation of transient receptor potential channel-related signature for predicting prognosis in patients with lung adenocarcinoma

SHENNAN HE, XIU FENG, YING CHEN and DIAN YIN

Department of Oncology, Nantong First People's Hospital and Second Affiliated Hospital of Nantong University, Nantong, Jiangsu 226014, P.R. China

Received March 17, 2025; Accepted July 4, 2025

DOI: 10.3892/ol.2025.15210

Abstract. Transient receptor potential (TRP) channels are central to human temperature detection and serve a crucial role in cancer development. However, their predictive potential in patients with lung adenocarcinoma (LUAD) remains unexplored. Differential expression analysis of TRP-related genes was performed using The Cancer Genome Atlas and validated using protein-protein interaction networks. Consensus clustering stratified the LUAD subtypes. A four-gene prognostic model of anillin (ANLN), cellular repressor of E1A stimulated genes 2 (CREG2), Ras homolog family member F, filopodia associated (RHOF) and CUB domain containing protein 1 was constructed using least absolute shrinkage and selection operator-Cox regression analysis and validated in Gene Expression Omnibus and IMvigor210 cohorts. Functional enrichment, immune microenvironment analysis and drug sensitivity prediction were performed. Reverse transcription-quantitative PCR demonstrated differential expression of the prognostic genes in a LUAD cell line. A total of 43 TRP-related differentially expressed genes were identified, with consensus clustering (k=2) revealing distinct survival subgroups (P=0.015). High-risk patients exhibited immunosuppressive microenvironments with reduced B-cell infiltration and lower immunotherapy response rates (P=0.021). Functional analysis demonstrated an association of high-risk profiles with mitotic cytokinesis and chemokine signaling. A total of eight chemotherapeutic agents showed differential sensitivity between risk groups. The model outperformed existing signatures using receiver operating characteristic area under the curve and concordance-index analyses. Experimental validation demonstrated elevated expression of ANLN, CREG2 and RHOF in LUAD cells, aligning with the bioinformatics findings. The present study identified a robust TRP channel-related four-gene signature as an independent prognostic biomarker for LUAD, offering insights into immune modulation and personalized therapeutic strategies. The model's predictive accuracy for survival and treatment response underscores its translational potential in clinical decision-making.

Correspondence to: Dr Dian Yin, Department of Oncology, Nantong First People's Hospital and Second Affiliated Hospital of Nantong University, 666 Shengli Road, Chongchuan, Nantong, Jiangsu 226014, P.R. China
E-mail: 6820648@qq.com

Abbreviations: LUAD, lung adenocarcinoma; PFS, progression-free survival; OS, overall survival; CI, confidence intervals; RFS, relapse free survival; HR, hazard ratio; TCGA, The Cancer Genome Atlas

Key words: transient receptor potential channel, lung adenocarcinoma, prognosis, signature

Introduction

Globally, lung cancer remains a leading cause of cancer mortality, with 2.2 million new cases and 1.8 million deaths annually (1). Prognosis is notably poor, demonstrating a 5-year survival rate of 10-20% globally and <7% for metastatic disease, largely due to late-stage diagnosis (2-4). Among its subtypes, lung adenocarcinoma (LUAD) is the most frequently diagnosed form of lung cancer. Despite previous advancements in the treatment of various cancers, the 5-year survival rate for lung cancer remains low (5). Consequently, identifying novel predictive gene signatures is crucial for improving prognosis and developing targeted therapeutic strategies for patients with LUAD.

The transient receptor potential (TRP) channels constitute a superfamily of non-selective cation channels that serve a pivotal role in calcium homeostasis and calcium-mediated signal transduction (6,7). Calcium-dependent signaling pathways are critical regulators of tumor cell survival, proliferation, invasiveness and therapeutic resistance, underscoring the importance of TRP channels as key modulators of carcinogenesis and tumor progression (8,9). Accumulating evidence suggests that tumors can markedly influence the expression and activation of TRP channels. Notably, specific subfamilies of TRP channels, including TRPV, TRPM and TRPC, have been strongly implicated in the initiation and progression of various cancers (10). For instance, TRPV4 has been shown to induce apoptosis in human lung cancer cells via the p38

MAPK pathway, highlighting its potential as a therapeutic target in lung cancer (11). Despite these advances, comprehensive bioinformatics analyses exploring the role of TRP channel-related genes in LUAD remain limited.

TRP channels are involved in both tumorigenesis and antitumor processes. However, their specific functions in LUAD remain poorly understood. To address this gap, a systematic investigation into the expression levels of TRP channel-related genes was performed in normal lung tissues compared with LUAD tissues. The present study aimed to explore the prognostic value of these genes and elucidate their potential connections with focal cell death and the tumor immune microenvironment.

However, the interaction between TRP channel dysregulation and immune cell infiltration in LUAD, a hallmark of tumor aggressiveness, remains uncharacterized. Therefore, the present study aimed to investigate the relationship between this TRP channel-related signature and the tumor immune microenvironment in LUAD, and to explore its potential clinical utility for therapeutic stratification. We employed comprehensive bioinformatic analyses combined with experimental validation to assess immune cell infiltration patterns associated with the signature and evaluate its implications for patient prognosis and treatment response.

Materials and methods

Datasets. RNA sequencing (RNA-seq) data from 535 patients with LUAD and 59 normal human lung tissues were obtained from The Cancer Genome Atlas (TCGA) database (TCGA-BRCA) (https://portal.gdc.cancer.gov/repository). The data were downloaded as raw counts and normalized to transcripts per million using the TCGAbiolinks R package (version 2.25.9) (12). Quality control steps included: i) Sample filtering, where patients with incomplete survival information or missing clinical annotations (such as tumor stage and age) were excluded; ii) batch effect correction where the ComBat algorithm from the sva R package (version 3.42.0) (13) was applied to adjust for batch effects across sequencing batches; and iii) gene expression filtering where genes with low expression (counts <10 in >90% of samples) were removed, retaining 19,856 protein-coding genes for downstream analysis.

For external validation, RNA-seq data (GSE50081) and clinical metadata from 127 patients with LUAD were retrieved from the Gene Expression Omnibus (GEO) database (https://www.ncbi.nlm.nih.gov/geo/) using the GEOquery R package (version 2.62.2) (14). Raw microarray data were normalized using robust multi-array average preprocessing using the limma R package (version 3.50.3) (15). Probes were annotated to gene symbols using the platform-specific annotation file (GPL570, Affymetrix Human Genome U133 Plus 2.0 Array).

Identification of differentially expressed TRP channel-associated genes. A total of 43 TRP channel-associated genes were identified using the following steps: i) GeneCards Database (https://www.genecards.org/): Genes were retrieved using the keyword 'TRP channel' and filtered by a relevance score ≥4.0 (top 20% high-confidence associations; score range, 0-10); i) Online Mendelian Inheritance in Man database (OMIM; https://www.omim.org/): Genes were selected based on experimental evidence (such as functional studies and cancer-related phenotypes) supporting direct roles in TRP channel activity or carcinogenesis; and iii) functional validation: Only genes encoding TRP channel proteins or directly regulating their activity (such as calcium transport and channel gating) were retained and indirect regulators were excluded. A full list of the 43 genes, including relevance scores, functional annotations and supporting references, is provided in Table SI.

Consensus clustering. Consensus clustering was performed using the k-means method to identify distinct TRP channel-related gene expression patterns. The optimal number of clusters and their stability were determined using the ConsensusClusterPlus R package (16). Clustering was repeated 1,000 times to ensure robustness.

Development and validation of the TRP channel-associated gene prognostic model. Differentially expressed genes (DEGs) between TRP channel-associated patterns were identified in TCGA cohort using an adjusted P-value of <0.05 and an absolute log2 fold change (log2FC) >1.5. The prognostic significance of TRP channel-associated genes was evaluated using Cox regression analysis. The least absolute shrinkage and selection operator (LASSO) method was applied to select and shrink variables. The risk score for each patient was calculated using the following formula: Risk score=(X1 x Y1) + (X2 x Y2) + (X3 x Y3) + (X4 x Y4), where X represents the regression coefficients and Y denotes the gene expression levels. Patients were stratified into high- and low-risk groups based on the median risk score.

Principal component analysis (PCA) and t-distributed stochastic neighbor embedding (t-SNE) were performed using the Rtsne (v0.17) (17) and ggplot2 (v3.5.1) (18) R packages, respectively, to visualize gene expression patterns (19). Time-dependent receiver operating characteristic (ROC) curve analysis was performed using the survival (v3.6-4) (20), timeROC (v0.4) (21) and survminer (v0.4.9) (22) R packages. The prognostic model was further validated using an independent LUAD cohort from the GEO database (GSE50081). Univariate and multivariate Cox regression analyses were performed to assess the predictive significance of the gene signature.

The prognostic utility of the risk model was further assessed using the IMvigor210 cohort, which included transcriptomic profiles and clinical outcomes of 348 patients with urothelial carcinoma receiving anti-PD-L1 therapy. Participants were stratified into four response categories: Complete response (CR), partial response (PR), stable disease (SD) and progressive disease (PD).

Functional enrichment analysis of DEGs between high- and low-risk groups. Functional enrichment analysis, including Gene Ontology (GO) and Kyoto Encyclopedia of Genes and Genomes (KEGG) pathway analyses, was performed using the clusterProfiler R package (v4.0.5) (23). Single-sample gene set enrichment analysis (ssGSEA) was performed using the GSVA package (v1.52.0) (24) to evaluate immune cell infiltration scores and the activity of immune-related pathways.

To investigate the association between signature genes (ANLN, CREG2, RHOF, CDCP1) and immune cell infiltration in LUAD, the TIMER database (http://timer.cistrome.org/) was used. Spearman correlation analysis was performed to evaluate the relationships between gene expression levels and immune cell infiltration abundances, including $CD8^+$ T cells, macrophages and other immune subsets.

Drug sensitivity prediction using the prophet algorithm. Drug response data (IC_{50} values) for LUAD cell lines were obtained from the publicly available Genomics of Drug Sensitivity in Cancer (GDSC) database (https://www.cancerrxgene.org/). The Prophet algorithm (25), a machine learning-based tool, was employed to model the relationship between the expression levels of the four-gene TRP channel-related signature and drug sensitivity. . Briefly, the input data of the gene expression profiles of ANLN, CREG2, RHOF and CDCP1 from TCGA-LUAD and GEO cohorts were normalized and integrated with GDSC-derived IC_{50} values. Prophet used a generalized additive model to regress gene expression against log-transformed IC_{50} values for model training, accounting for non-linear relationships and interaction effects. The model was internally validated using 10-fold cross-validation within TCGA cohort. Predictive accuracy was assessed using Pearson correlation between predicted and observed IC_{50} values.

Cell culture. The LUAD cell line H1299 (Shaanxi Fuheng Biotechnology Co., Ltd.), and normal bronchial epithelial cells, BEAS-2B (BeNa Culture Collection), were used in the present study. H1299 cells were cultured in RPMI-1640 medium (Gibco; Thermo Fisher Scientific, Inc.) supplemented with 10% fetal bovine serum (FBS; Gibco; Thermo Fisher Scientific, Inc.) and 1% penicillin/streptomycin (HyClone™; Cytiva), while BEAS-2B cells were maintained in Bronchial Epithelial Cell Growth Medium (BEGM; Lonza Group Ltd.) containing the manufacturer's recommended supplements (BEGM BulletKit; Lonza). Both cell lines were incubated at 37˚C in a humidified 5% CO_2 atmosphere and passaged using 0.25% trypsin-EDTA (Gibco; Thermo Fisher Scientific, Inc.). Mycoplasma contamination was routinely excluded using the MycoAlert™ Detection Kit (Lonza Group Ltd.).

Reverse transcription (RT)-quantitative (q)PCR. For RT-qPCR validation, total RNA was extracted from cells using TRIzol® reagent (Invitrogen; Thermo Fisher Scientific, Inc.), and RNA purity was verified using a NanoDrop 2000 spectrophotometer (Thermo Fisher Scientific, Inc.). Reverse transcription was performed with 1 μg RNA using the PrimeScript™ RT Reagent Kit (Takara Bio, Inc.), followed by qPCR amplification using a QuantStudio 5 System (Applied Biosystems; Thermo Fisher Scientific, Inc.) with TB Green® Premix Ex Taq™ II (Takara Bio, Inc.). The thermal profile included an initial denaturation at 95˚C for 30 sec, 40 cycles at 95˚C for 5 sec and 60˚C for 34 sec and melt curve analysis. Gene expression levels were normalized to β-actin using the $2^{-\Delta\Delta Cq}$ method (26), with triplicate technical replicates (27). Primer sequences were as follows: β-actin-forward (F) 5'-GCACCACACCTTCTACAATGAGC-3', β-actin-reverse (R) 5'-GGATAGCACAGCCTGGATAGCAAC-3', ANLN-F 5'-ACTCAGTCACTTCCAGTAACAG-3', ANLN-R 5'-GCTAGATTTCGTCATTTCGCAT-3', CREG2-F 5'-ATGAAGAACCCCATGGCCTC-3', CREG2-R, 5'-AAAACATGGCTTGCTTGGCA-3', RHOF-F, 5'-CTCCTTCCCCGAGCACTACG-3', RHOF-R 5'-TAGCAGATGAGCACGAGGTG-3', CDCP1-F 5'-CAACATCAATACTGAGATGCCG-3', CDCP1-R 5'-GTAGCAGATGCCCATATACCAT-3'.

Statistical analysis. All statistical analyses were performed using R software (version 4.1.2; R Foundation for Statistical Computing). Data are presented as mean ± SEM. Comparisons between normal and tumor groups were performed using an unpaired two-tailed Student's t-test (n=3 independent experiments). $P<0.05$ was considered to indicate a statistically significant difference.

Results

Identification of TRP-related DEGs in LUAD. A Venn diagram revealed that 66 TRP channel-related genes were identified as the intersection between the GeneCards and OMIM databases (Fig. 1A). Expression levels of these 66 genes were compared between 59 normal lung tissues and 535 LUAD tissues from TCGA database, leading to the identification of 43 DEGs (Fig. 1B). To further explore the interactions among these TRP channel-related genes, a protein-protein interaction (PPI) network was constructed (Fig. 1C), and the correlation network of these genes was visualized (Fig. 1D).

Subgroups of LUAD identified by TRP channel-encoding genes. To investigate the relationship between the 43 TRP channel-encoding DEGs and LUAD subtypes, consensus clustering analysis was performed on 535 patients with LUAD from TCGA cohort. The optimal number of clusters (k=2) was determined based on clustering stability (Fig. 2A). Patients in Cluster 2 exhibited significantly shorter overall survival (OS) compared with those in Cluster 1 ($P=0.015$; Fig. 2B). A heatmap displaying gene expression profiles and clinical parameters (such as age, stage and sex) revealed that sex was a distinguishing factor between the two clusters (Fig. 2C).

Prognostic model construction and validation. Univariate Cox regression analysis was used to identify survival-associated genes (Fig. 3A). A four-gene TRP channel-related signature was developed using LASSO Cox regression analysis, with the optimal λ value selected (Fig. 3B and C). The risk score was calculated as follows: Risk score=(0.102 x ANLN expression) + (0.114 x CREG2 expression) + (0.001 x RHOF expression) + (0.004 x CDCP1 expression).

Patients were stratified into high- and low-risk groups based on the median risk score. The risk stratification model effectively segregated patients into high- and low-risk prognostic groups, with higher risk scores predominantly assigning patients to the high-risk category and lower scores to the low-risk category (Fig. 4A and C). PCA and t-SNE demonstrated distinct clustering patterns between the risk groups (Fig. 4E and G). Time-dependent ROC analysis revealed that the 1-, 3- and 5-year area under the curve (AUC) values for the risk score were 0.679, 0.669 and 0.628, respectively (Fig. 5A). High-risk patients exhibited significantly shorter survival times compared with low-risk patients ($P<0.001$; Fig. 5C).

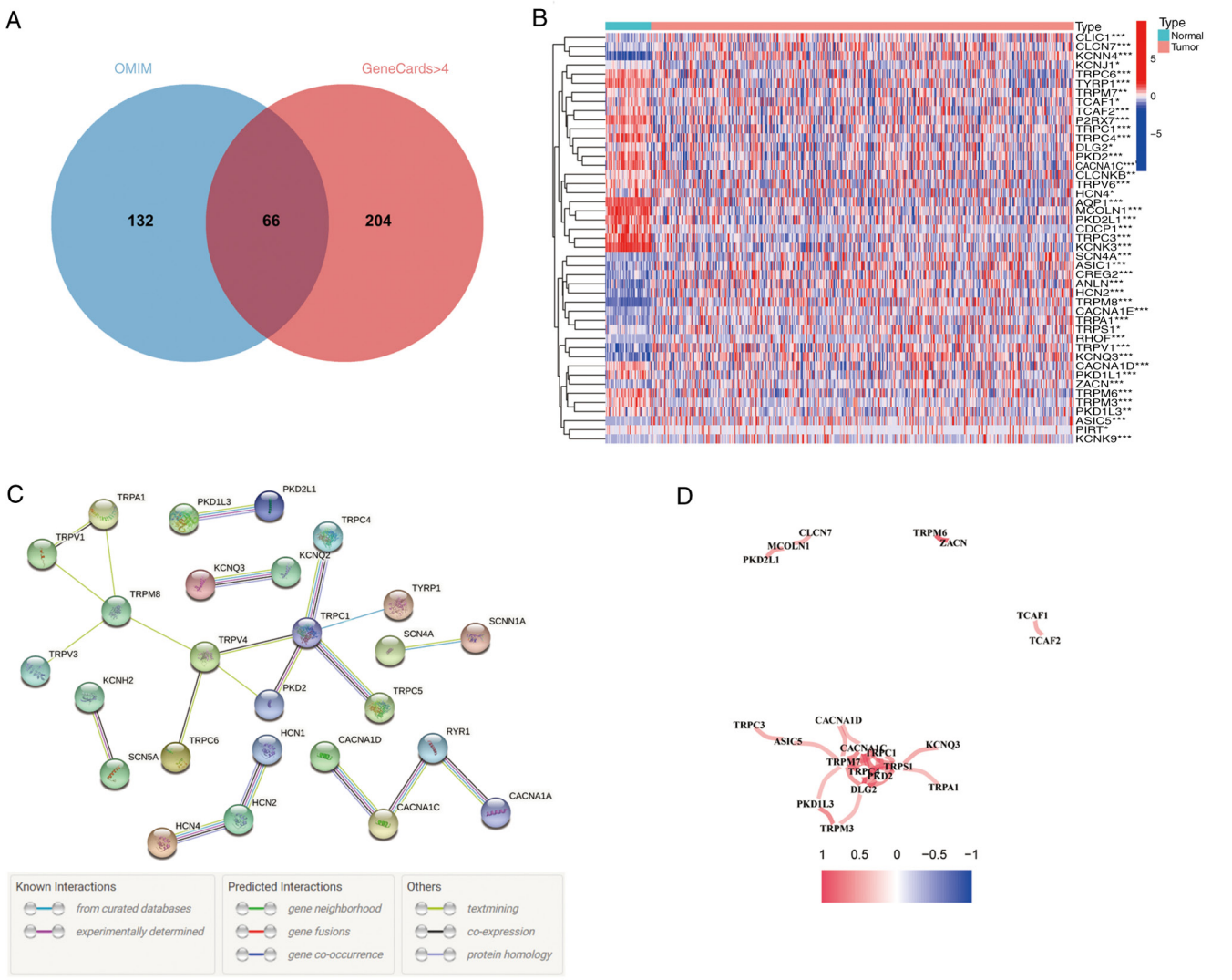

Figure 1. Differential expressions of the 43 TRP channel-related genes and the interactions among them. (A) Identification of the TRP channel-related genes by taking an intersection of the results from GeneCards database (relevance score >4) and OMIM database. (B) Heatmap depicting the variations in expression of 43 TRP channel-related genes between the normal and tumor samples. P-values are shown as *P<0.05; **P<0.01; ***P<0.001. (C) Protein-protein interaction network showing the interactions of the TRP channel-related genes (interaction score=0.9). (D) The correlation network of the TRP channel-related genes. The red line indicates a positive correlation and the depth of the colors reflects the strength of the relevance. OMIM, Online Mendelian Inheritance in Man; TRP, transient receptor potential.

Validation of the four-gene TRP channel-related signature in the GEO cohort. The prognostic model was validated using an independent LUAD cohort from the GEO database. Patients were stratified into high- and low-risk groups based on the median risk score derived from TCGA cohort. The risk stratification model demonstrated discriminative capacity for patient survival outcomes (Fig. 4B and D). PCA and t-SNE analyses further supported the distinct clustering of risk groups (Fig. 4F and H). Time-dependent ROC analysis showed AUC values of 0.616, 0.627 and 0.724 for 1-, 3- and 5-year survival, respectively (Fig. 5B). High-risk patients had significantly shorter survival times compared with low-risk patients (P<0.042; Fig. 5D).

Independent prognostic value of the four-gene TRP channel-related signature. The risk score independently predicted poor survival in both TCGA [hazard ratio (HR)=10.1; 95% confidence interval (CI), 4.6-22.3] and GEO cohorts (HR=7.5; 95% CI, 1.8-32.2; univariate Cox), which remained significant after multivariate adjustment (TCGA, HR=6.3; 95% CI, 2.7-15.1; GEO, HR=8.2; 95% CI, 1.7-39.4) (Fig. 6A-D). A heatmap of clinicopathological characteristics and gene expression profiles further illustrated the differences between high- and low-risk subgroups (Fig. 6E). High-risk patients in the IMvigor210 cohort exhibited significantly worse overall survival compared with the low-risk group (HR=1.8; 95% CI, 1.2-2.7; P=0.038; Fig. 6F), demonstrating the prognostic value of the TRP channel-related signature in an immunotherapy context. Patients achieving objective responses (CR/PR) had significantly lower risk scores compared with non-responders (SD/PD; P=0.021; Fig. 6G), suggesting that the signature predicts not only survival but also therapeutic efficacy. ROC analysis demonstrated moderate predictive accuracy for immunotherapy response (AUC=0.592; 95% CI, 0.516-0.667; Fig. 6H), highlighting the potential of the risk score as a standalone biomarker despite multifactorial resistance mechanisms.

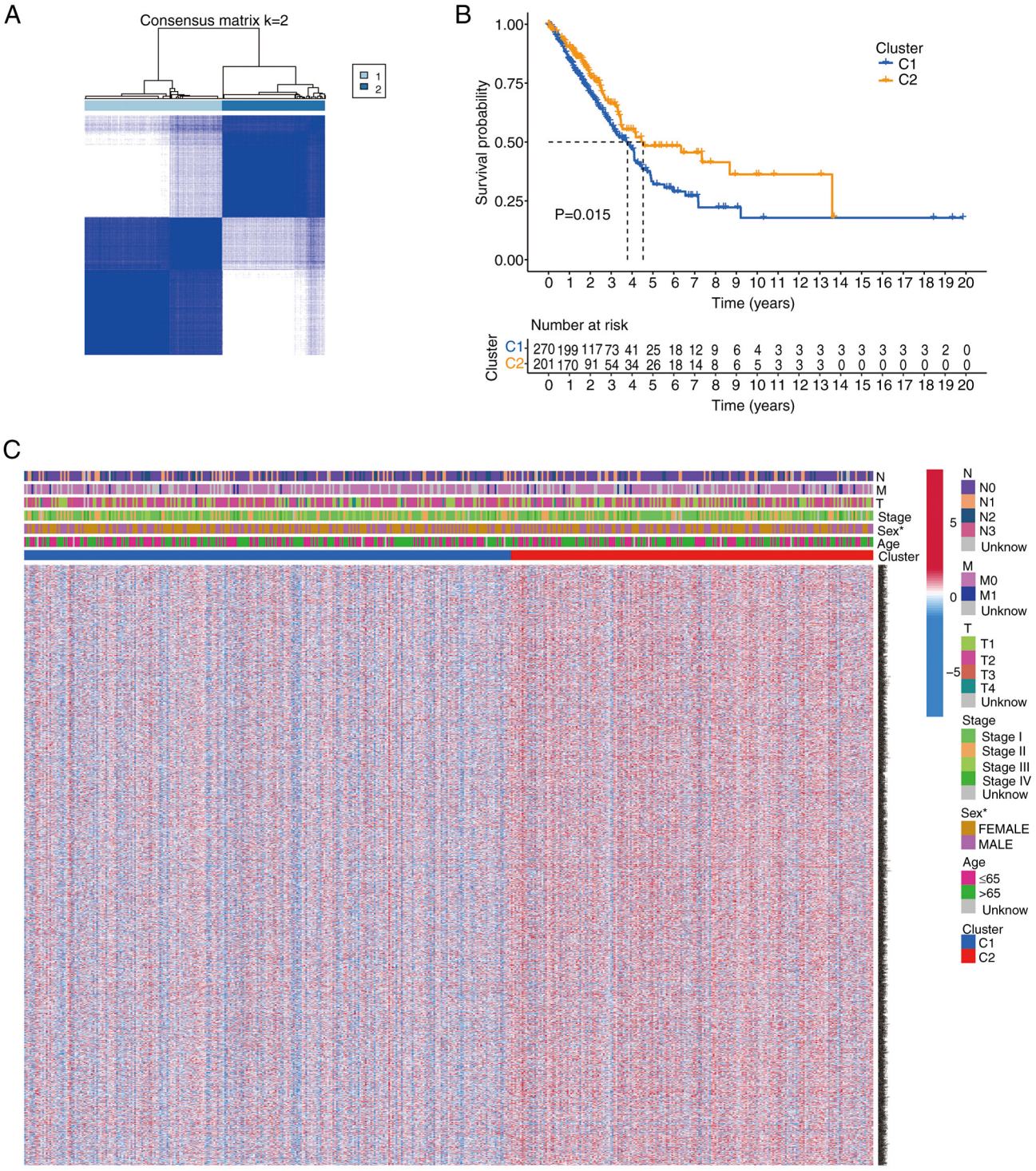

Figure 2. Subgroups of LUAD defined by genes involved in TRP channel. (A) TCGA cohort's consensus score matrix for all samples when k=2. When two samples had a higher consensus score in distinct interactions, they were more likely to be clustered together. (B) Overall survival curves based on patients with LUAD from TCGA cohort for the two TRP channel-related clusters. (C) Consensus clustering of differentially expressed genes in TCGA cohort's two TRP channel-related clusters. *P<0.05. LUAD, lung adenocarcinoma; TRP, transient receptor potential; TCGA, The Cancer Genome Atlas; T, tumor stage; N, lymph node stage; M, metastasis stage.

To facilitate clinical translation, a nomogram was constructed incorporating the risk score, age, TNM stage and sex (Fig. S1A). Each variable was assigned a weighted point contribution, with the risk score showing the strongest prognostic impact. Calibration plots demonstrated notable concordance between predicted and observed survival rates at 1, 3 and 5 years (Fig. S1B).

Functional analysis of DEGs between high- and low-risk groups. Functional enrichment analysis of DEGs (log2FC >1.5; false discovery rate <0.05) revealed significant associations with cellular processes, environmental information processing, genetic information processing and human diseases in KEGG analysis (Fig. 7B). GO analysis highlighted pathways associated with mitotic cytokinesis and protein signal transduction (Fig. 7A).

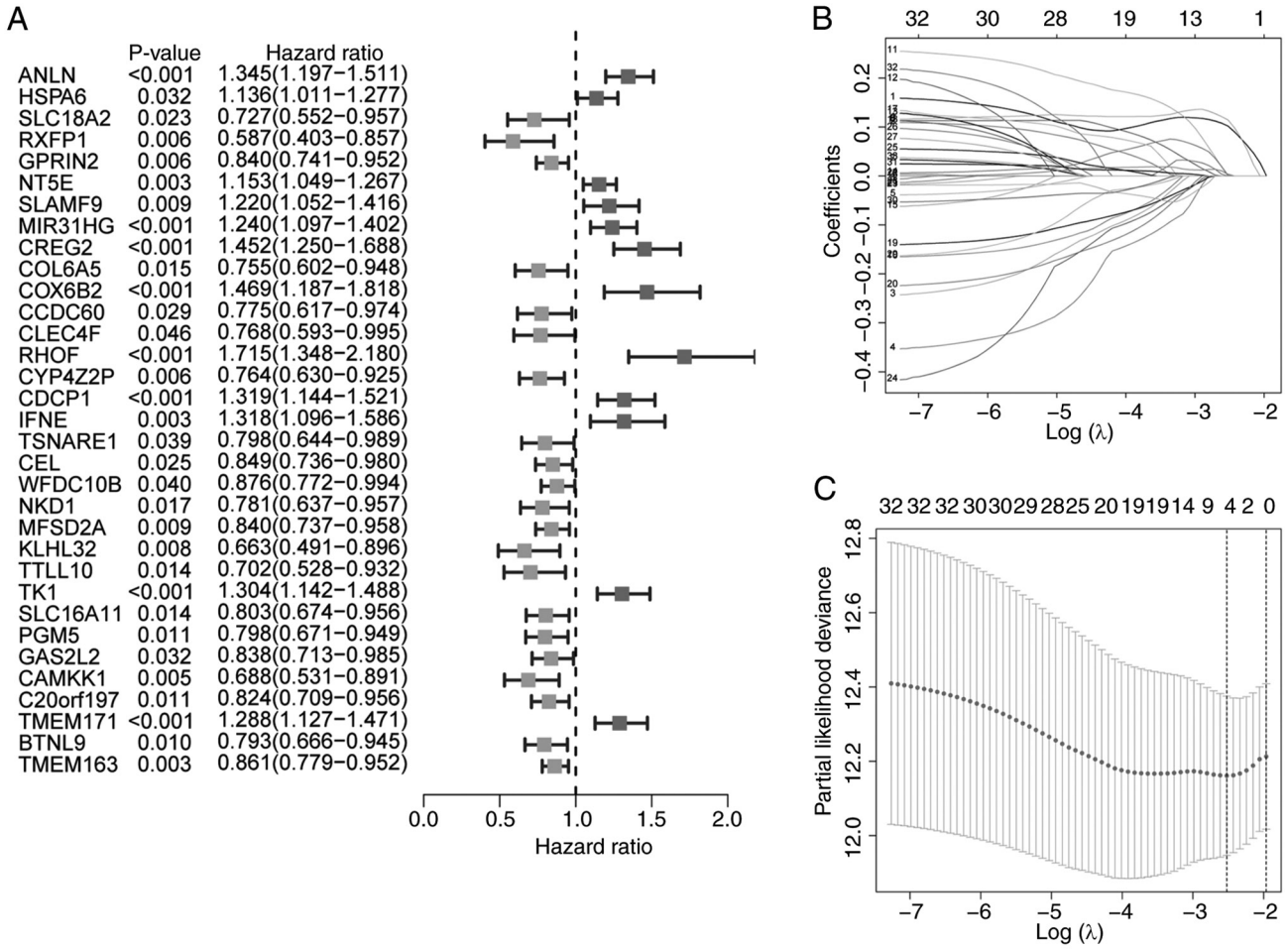

Figure 3. Prognostic gene signature development using LASSO Cox regression. (A) Forest plot showing the results of the univariate Cox-regression analysis between differentially expressed genes expression and overall survival with 8 genes with a P-value <0.001. (B) Coefficient profiles of genes during LASSO regularization. (C) Partial likelihood deviance (solid line, left axis) and number of non-zero coefficients (dotted line, right axis) versus log(λ). The optimal log(λ) (vertical dashed line) was chosen using the minimum deviance+1 standard error rule. The top axis shows the corresponding Hazard Ratio scale.

Immune microenvironment and therapeutic implications. ssGSEA revealed elevated immune cell infiltration, including higher levels of B cells and tumor-infiltrating lymphocytes (TILs), in the low-risk subgroup compared with the high-risk subgroup within TCGA cohort (Fig. 8A). Functional immune profiling further demonstrated enhanced activity of chemokine-mediated signaling ('CCR') and 'parainflammation' pathways in the low-risk group (Fig. 8B), with consistent trends observed in the GEO cohort (Fig. 8C and D). To investigate the role of TRP channel-related genes in immune regulation, their associations with immune cell infiltration were analyzed using the TIMER database. Notably, the TRP channel-related signature exhibited a significant negative correlation with B cell infiltration ($P<0.05$), suggesting potential suppression of B cell recruitment via specific regulatory pathways. Collectively, these findings underscore the dual role of TRP channel-related signatures in shaping both pro-inflammatory and immunosuppressive microenvironments (Fig. S2).

Response to treatment in high- and low-risk groups. The Prophet algorithm was used to predict chemotherapy response based on the IC_{50}. A total of eight small-molecule compounds, including bexarotene, ispinesib, pyrimethamine, tipifarnib, etoposide, paclitaxel, ruxolitinib and vinorelbine, showed significant differences in sensitivity between high- and low-risk groups (Fig. 9).

The ROC curve and concordance (C)-index were used to compare the models. The prognostic model was compared with three previously published LUAD signatures (28-30). The AUC and C-index values of the present model were superior to those of the other models (Fig. 10A and B).

Validation of the four-gene TRP channel-related signature expression in LUAD cells. RT-qPCR analysis demonstrated that the mRNA expression levels of ANLN, CREG2 and RHOF were significantly higher in the LUAD cell line (H1299) compared with the normal lung cell line (BEAS-2B), while CDCP1 expression was lower (Fig. 11A). Immunohistochemical analysis further validated these findings at the protein level (Fig. 11B), consistent with the mRNA expression results. To further validate the expression trends, RNA-seq data from the Cancer Cell Line Encyclopedia (CCLE) were analyzed. Among 30 cancer cell lines, ANLN, CREG2 and RHOF genes exhibited significantly higher expression levels in LUAD cells, while the CDCP1 gene displayed a low expression pattern (Fig. S3). This pan-cell line consistency reinforces the reliability of the signature.

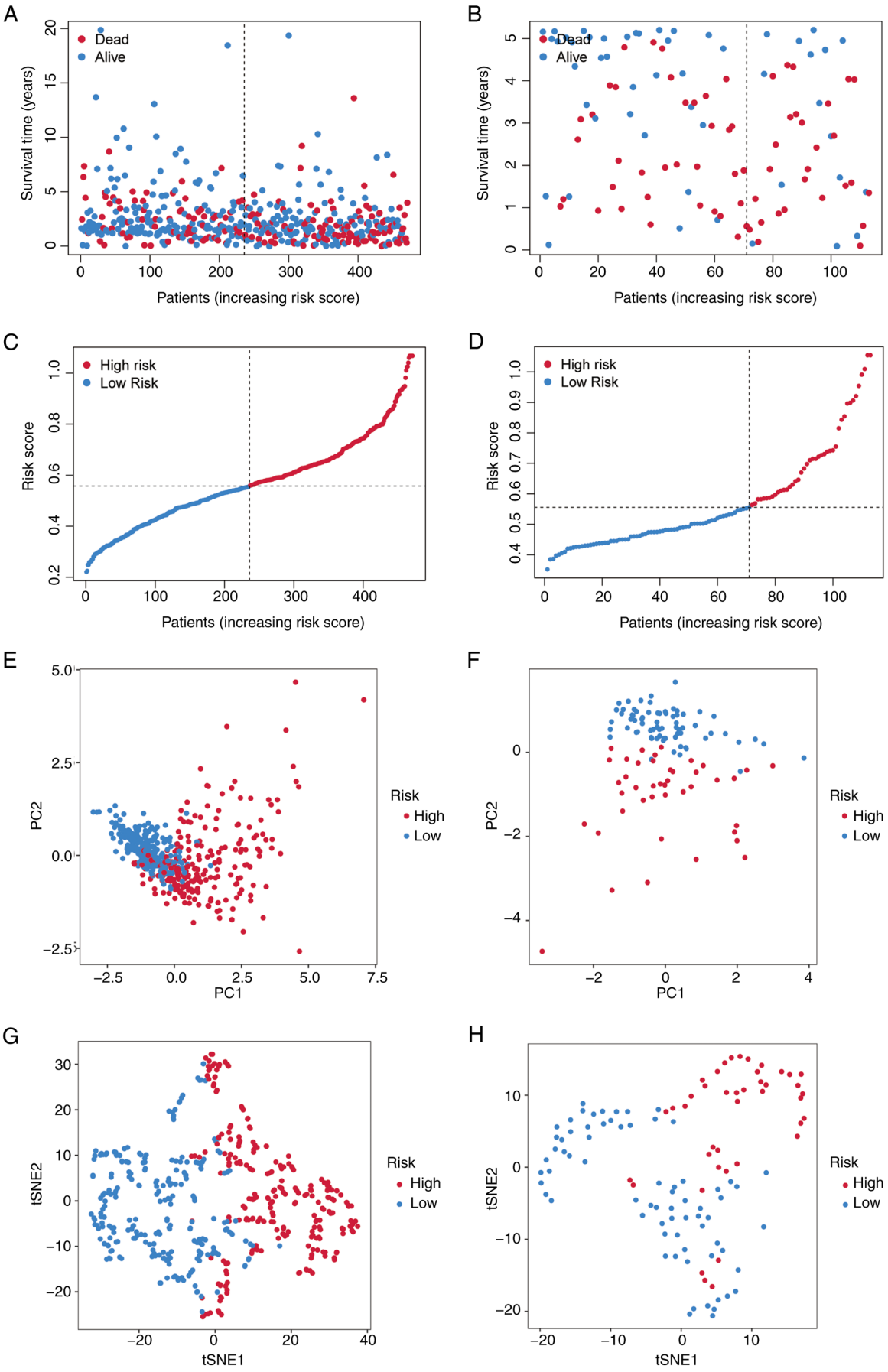

Figure 4. Data distribution of prognostic model using TGCA and GEO databases. (A) Distribution of operating system status in TGCA. (B) The distribution of operating system status in GEO databases. (C) The risk scores' median value and dispersion in TGCA. (D) The risk scores' median value and dispersion in TGCA. (E) Plot of principal component analysis in TGCA. (F) Plot of principal component analysis GEO databases. (G) Examination of the t-SNE coefficients in TGCA. (H) t-SNE coefficients in GEO databases. TCGA, The Cancer Genome Atlas; GEO, gene expression omnibus.

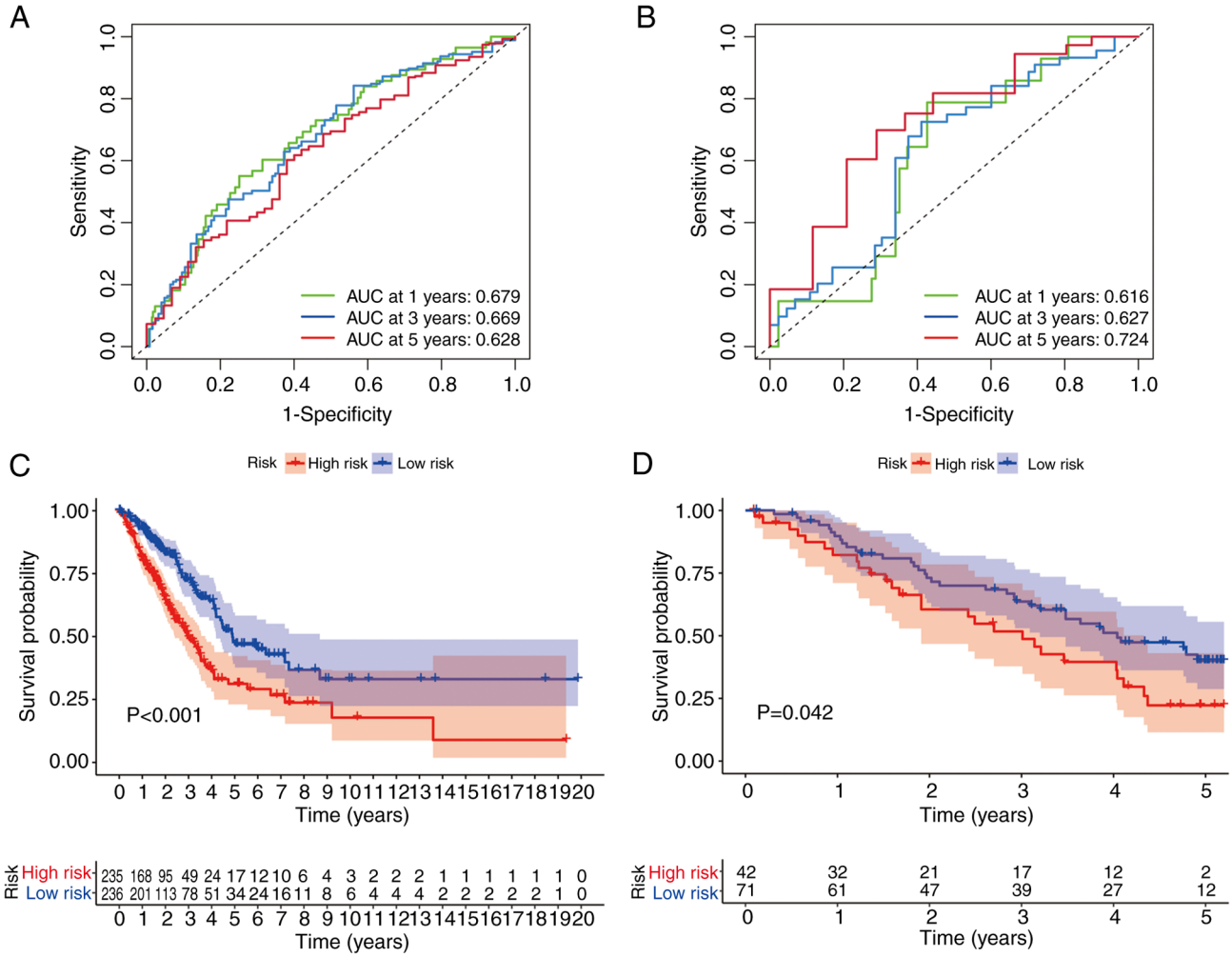

Figure 5. Development of a gene signature to predict patient OS based on clusters associated with TRP channel. (A) Time-dependent ROC analysis of the risk score in TCGA cohort. (B) Time-dependent ROC analysis of the risk score in the GEO cohort. (C) OS curves for TCGA cohort's various risk score subgroups. (D) Overall survival curves for the GEO cohort's various risk score subgroups. OS, overall survival, TCGA, The Cancer Genome Atlas; t-SNE2, t-distributed stochastic neighbor embedding; PC, principal component; GEO, gene expression omnibus; ROC, receiver operating characteristic; AUC, area under the curve.

Discussion

The present study aimed to investigate the expression levels of TRP channel-related genes in LUAD, their prognostic significance and their role in the tumor microenvironment. Compared with normal tissues, LUAD tissues exhibited significantly elevated expression of ANLN, CREG2 and RHOF, while CDCP1 expression was markedly reduced. Using consensus clustering based on the expression profiles of 43 TRP channel-associated DEGs, two distinct LUAD subgroups were identified: Cluster 1 and Cluster 2. Patients in Cluster 2 were associated with early tumor stage and grade, while Cluster 1 patients exhibited a lower probability of survival.

A prognostic risk score model was developed for the TCGA-LUAD cohort, incorporating four TRP channel-related genes (ANLN, CREG2, RHOF and CDCP1). This model effectively stratified patients with LUAD into low- and high-risk groups, with low-risk patients demonstrating markedly improved survival outcomes. The prognostic utility of this signature was further validated in an independent GEO-LUAD cohort. Notably, the risk score increased progressively with tumor progression, and both univariate and multivariate Cox regression analyses confirmed the four-gene signature as an independent prognostic factor.

Among the four genes, ANLN, a scaffold protein critical for cytokinesis, is overexpressed in LUAD and promotes tumor proliferation through PI3K/Akt activation (31,32). RHOF, a Rho GTPase regulating cytoskeletal dynamics and epithelial-mesenchymal transition (EMT), was also identified as a key player (33). Both genes were upregulated in high-risk patients. Consistent with these findings, pathway analysis revealed significant enrichment of PI3K-Akt signaling and cell cycle pathways, thereby supporting their mechanistic roles in mitotic dysregulation and tumor progression.

CREG2, a secreted glycoprotein involved in pluripotent stem cell differentiation (34), has not been previously studied in LUAD. CREG2 regulates angiogenesis and immune responses by modulating VEGF and TGF-β pathways (35). High CREG2 expression was protective in the present model. KEGG analysis highlighted suppressed angiogenesis pathways (such as VEGF signaling) in high-risk patients, consistent with the role of CREG2 in maintaining vascular homeostasis. This implies that CREG2 downregulation may impair antitumor

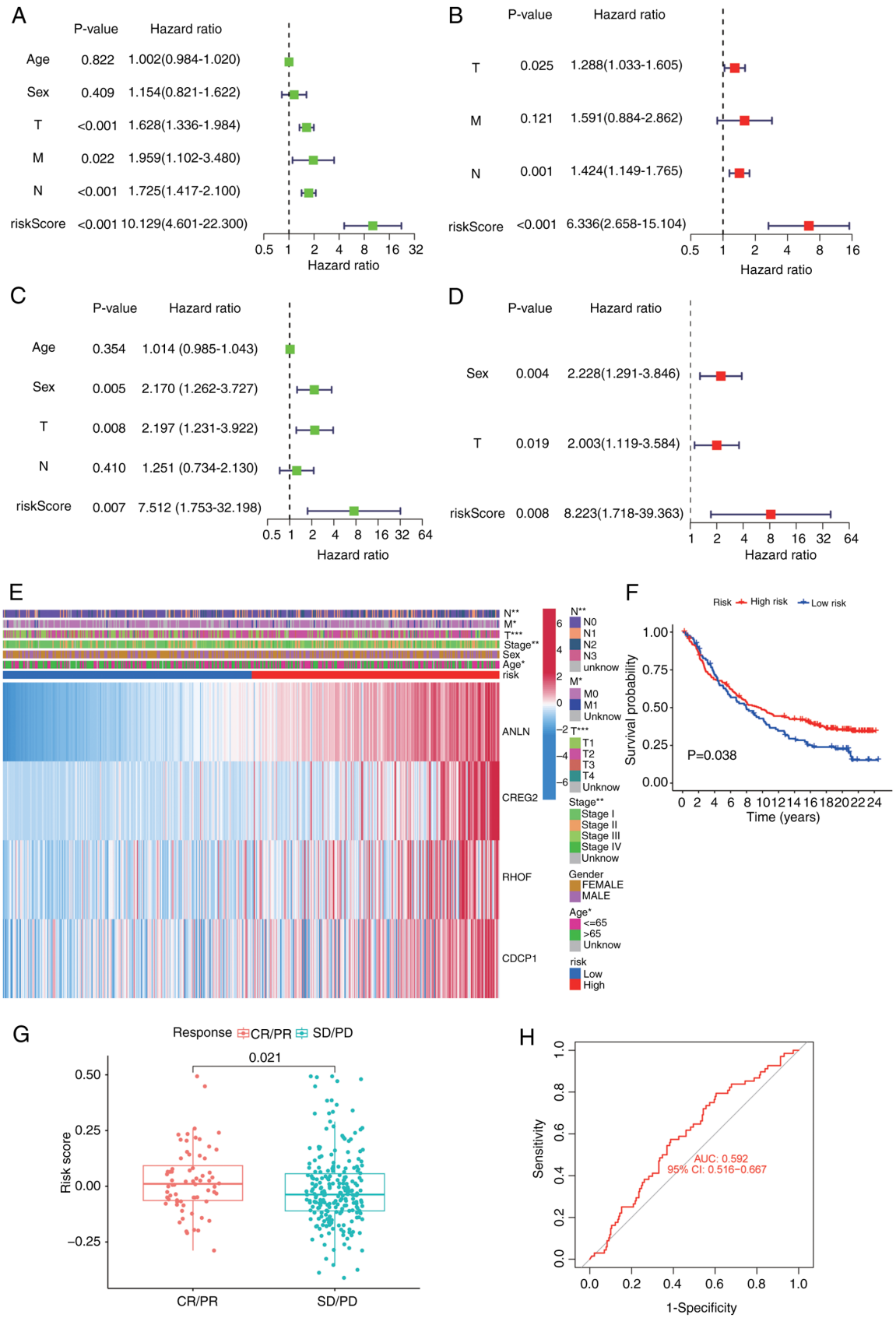

Figure 6. Univariate and multivariate Cox regression analyses for the risk score. (A) TCGA univariate independent prognostic analysis results. (B) TCGA multifactor independent prognostic analysis results. (C) GEO univariate independent prognostic analysis results. (D) GEO multifactor independent prognostic analysis results. (E) Heatmap depicting the clinicopathological characteristics and gene expression variations between the high-risk and low-risk groups. (F) Kaplan-Meier survival curves for high- and low-risk groups in the IMvigor210 cohort (P=0.038). (G) Risk score distribution in IMvigor210 patients stratified by immunotherapy response (CR/PR vs. SD/PD). (H) Receiver operating characteristic curve evaluating the risk score's ability to predict immunotherapy response (AUC=0.592). *P<0.05; **P<0.01; ***P<0.001. TCGA, The Cancer Genome Atlas; GEO, gene expression omnibus; CR, complete response; PR, partial response; SD, stable disease; PD, progressive disease; CI, confidence interval; ANLN, anillin; CREG2, cellular repressor of E1A stimulated genes 2; RHOF, Ras homolog family member F, filopodia associated; CDCP1, CUB domain containing protein 1; T, tumor stage; N, lymph node stage; M, metastasis stage.

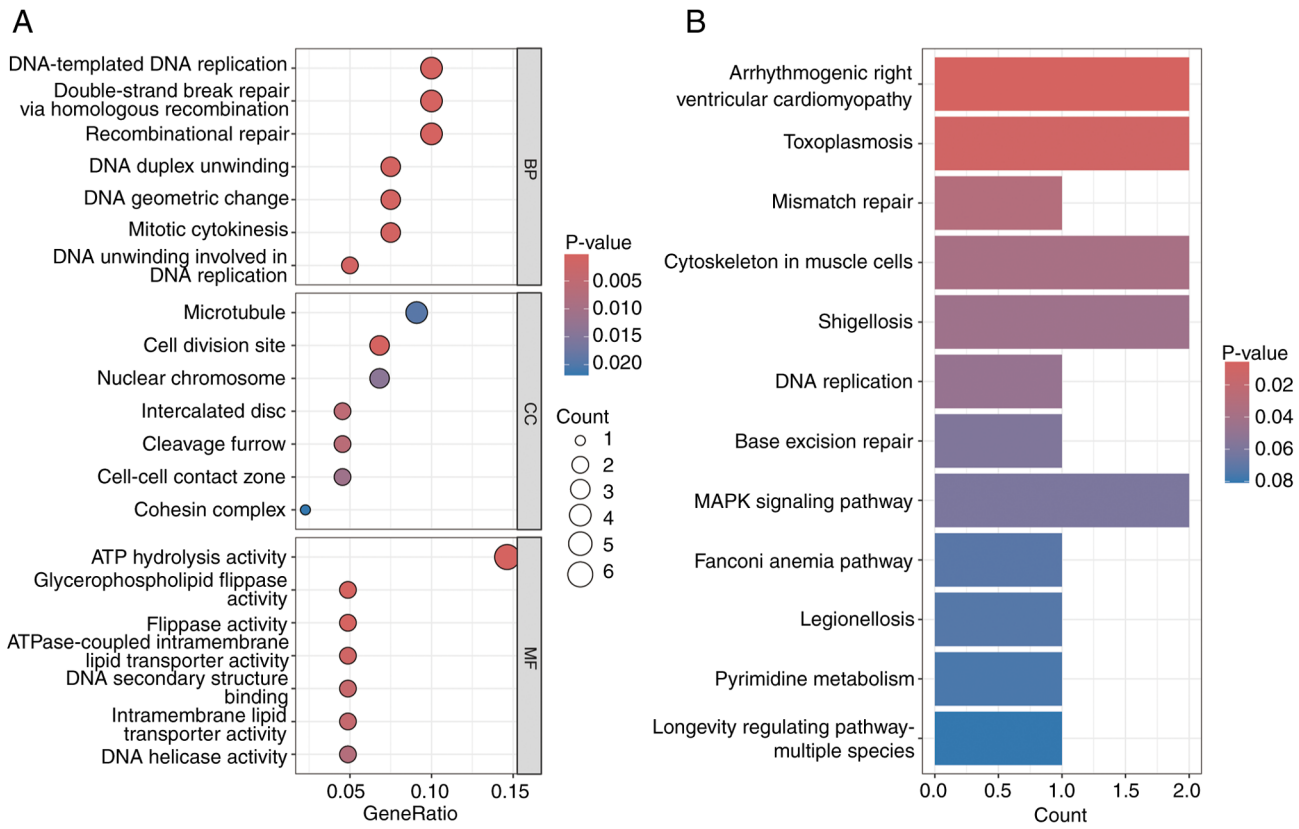

Figure 7. Functional analysis based on the differentially expressed genes between the two-risk groups in TCGA cohort. (A) Bubble of Gene Ontology analyses for differentially expressed genes among high and risk groups based on TCGA (the bubble size indicates the number of genes enriched and the color indicates the P-value). (B) Bar plot of Kyoto Encyclopedia of Genes and Genomes analyses for differentially expressed genes among high and risk groups based on TCGA (the bar length indicates the number of enriched genes, while the colors indicate the P-value). TCGA, The Cancer Genome Atlas; BP, biological process; CC, cellular component; MF, molecular function.

immunity and promote hypoxia-driven progression. CDCP1 is a transmembrane protein that promotes metastasis in multiple cancers by activating Wnt/β-catenin signaling and EMT (36). In the model, low CDCP1 expression was associated with poor prognosis, aligning with its reported role in suppressing LUAD metastasis (37,38). Pathway analysis revealed significant downregulation of Wnt signaling in high-risk patients, suggesting that CDCP1 loss may drive aggressive phenotypes via Wnt pathway inactivation. These findings underscore the importance of TRP channel-related genes in cancer biology.

TRP channels are critical regulators of intracellular calcium homeostasis, which is essential for immune cell activation and cytokine production (39). The ssGSEA results revealed significantly higher infiltration of B cells and TILs in the low-risk group. This aligns with previous studies showing that TRP channel-mediated calcium influx promotes T-cell receptor signaling and B-cell differentiation. For instance, TRPV1 activation enhances cytotoxic T-cell activity by upregulating IFN-γ secretion (40), while TRPM2 inhibition suppresses regulatory T-cell function, thereby reducing immune suppression (41). The upregulation of CDCP1 (a negative regulator of TRPC6) in high-risk patients may impair calcium-dependent T-cell activation, contributing to the observed immunosuppressive microenvironment. The IMvigor210 analysis extends the findings beyond chemotherapy, implicating TRP channel dysregulation in immunotherapy resistance. The association between low-risk scores and improved PD-L1 response may stem from enhanced immune infiltration, a hypothesis supported by elevated $CD8^+$ T-cell levels and IFN-γ signaling in low-risk patients.

The low-risk group exhibited stronger activity in CCR pathways. TRP channels, particularly TRPC and TRPV subfamilies, regulate chemokine receptor expression and immune cell chemotaxis (42). For example, TRPV4 activation in endothelial cells facilitates leukocyte transmigration by upregulating C-X-C motif chemokine (CXC) ligand 12/CXC receptor type 4 signaling (43). The downregulation of RHOF (a Rho GTPase associated with TRPM7) in low-risk patients may enhance dendritic cell migration via cytoskeletal remodeling, promoting antigen presentation and TIL recruitment (44).

Parainflammation, a state of chronic, low-grade inflammation, was more pronounced in the low-risk group compared with the high-risk group. TRP channels such as TRPA1 and TRPV1 are known to mediate neurogenic inflammation by releasing pro-inflammatory neuropeptides (45). In LUAD, sustained TRP channel activation may drive parainflammation, paradoxically favoring immune surveillance by recruiting natural killer cells and M1 macrophages (46). Conversely, high-risk patients showed reduced parainflammation, potentially due to ANLN overexpression, which has been associated with immunosuppressive cytokine secretion and macrophage polarization toward the M2 phenotype.

Drug susceptibility analysis suggested that high-risk patients may exhibit favorable responses to specific chemotherapy agents, such as bexarotene, ispinesib and paclitaxel.

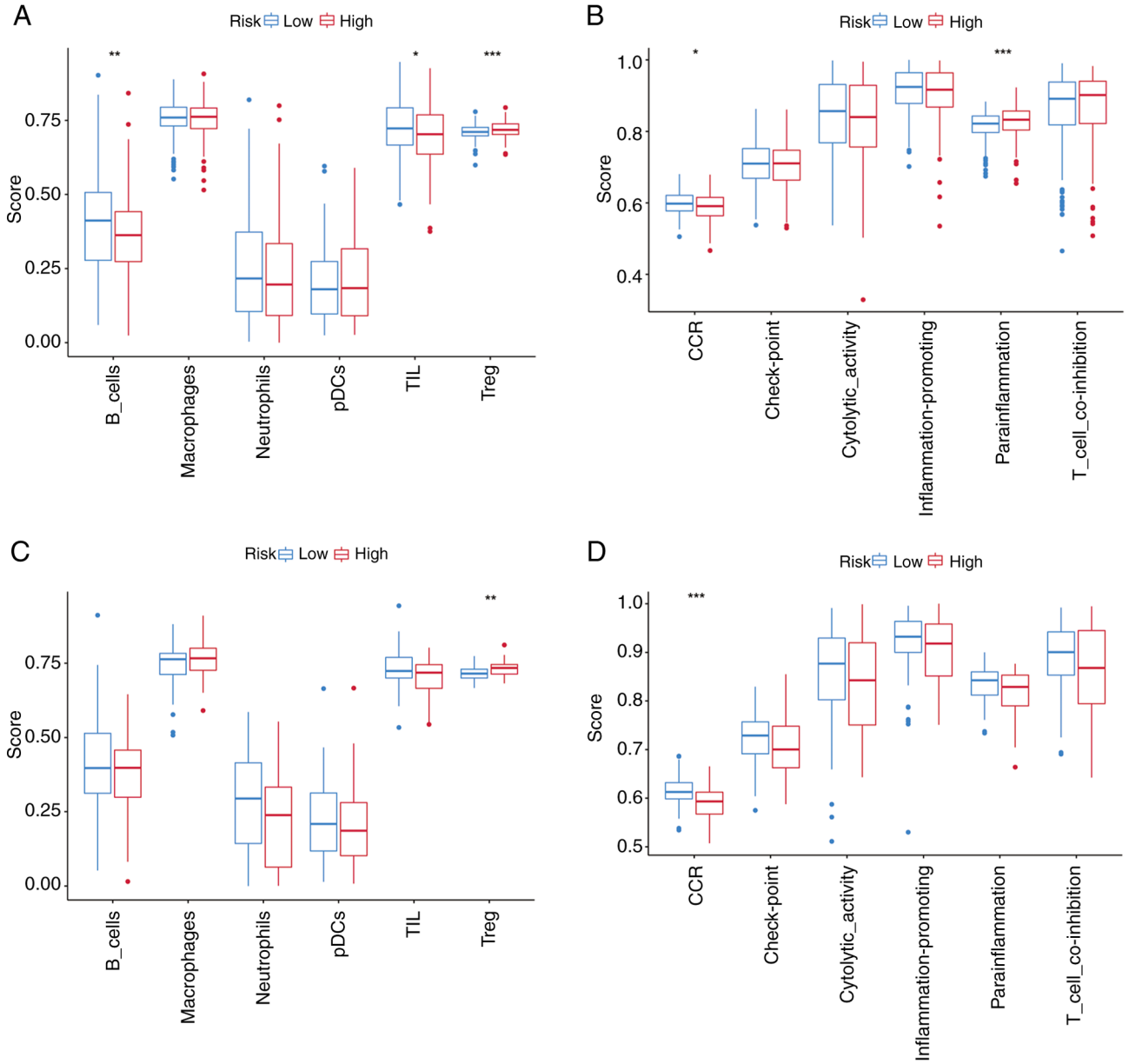

Figure 8. Comparison of the single-sample gene set enrichment analysis scores for immune cells and immune pathways. Comparison of the enrichment scores of (A) six types of immune cells and (B) six immune-related pathways between low- (blue box) and high-risk (red box) groups in The Cancer Genome Atlas cohort. Comparison of (C) immune cells and (D) immune-related pathways between low- (blue box) and high-risk (red box) groups in the Gene Expression Omnibus cohort. P-values are shown as *P<0.05; **P<0.01; ***P<0.001. pDCs, plasmacytoid dendritic cells; TIL, tumor-infiltrating lymphocytes; Treg, regulatory T cells; CCR, chemokine-mediated signaling.

These findings highlight the potential of TRP channel-related genes as predictive biomarkers for therapeutic efficacy in patients with LUAD.

Previous studies have advanced the understanding of TRP-related biology in LUAD, including a 12-gene immune-focused model (47), a five-gene tryptophan metabolism signature (48) and an eight-gene cytokine-centric model (49). While these studies established the prognostic value of TRP-associated pathways, the present study provides critical distinctions. Firstly, a minimalist four-gene signature focused on TRP channel-encoding genes was developed, avoiding overfitting while achieving superior accuracy (AUC, 0.679-0.724). Secondly, the signature introduces novel biomarkers (CREG2, CDCP1) not previously associated with LUAD, expanding the mechanistic scope of TRP biology to include angiogenesis and metastasis suppression. Thirdly, the model's utility in predicting anti-PD-L1 response was validated using the IMvigor210 cohort, bridging TRP dysregulation to immunotherapy resistance, a finding absent in prior studies. Finally, the integration of multi-omics validation (CCLE and cell lines) and clinical translation tools (nomogram) addresses limitations of earlier bioinformatics-centric approaches, offering a robust framework for personalized prognosis.

Despite these insights, the present study has several limitations. First, the sample size and training cohort for the prognostic model were relatively modest, which may affect the generalizability of the findings. Second, additional clinical data are needed to further validate the nomogram and enhance

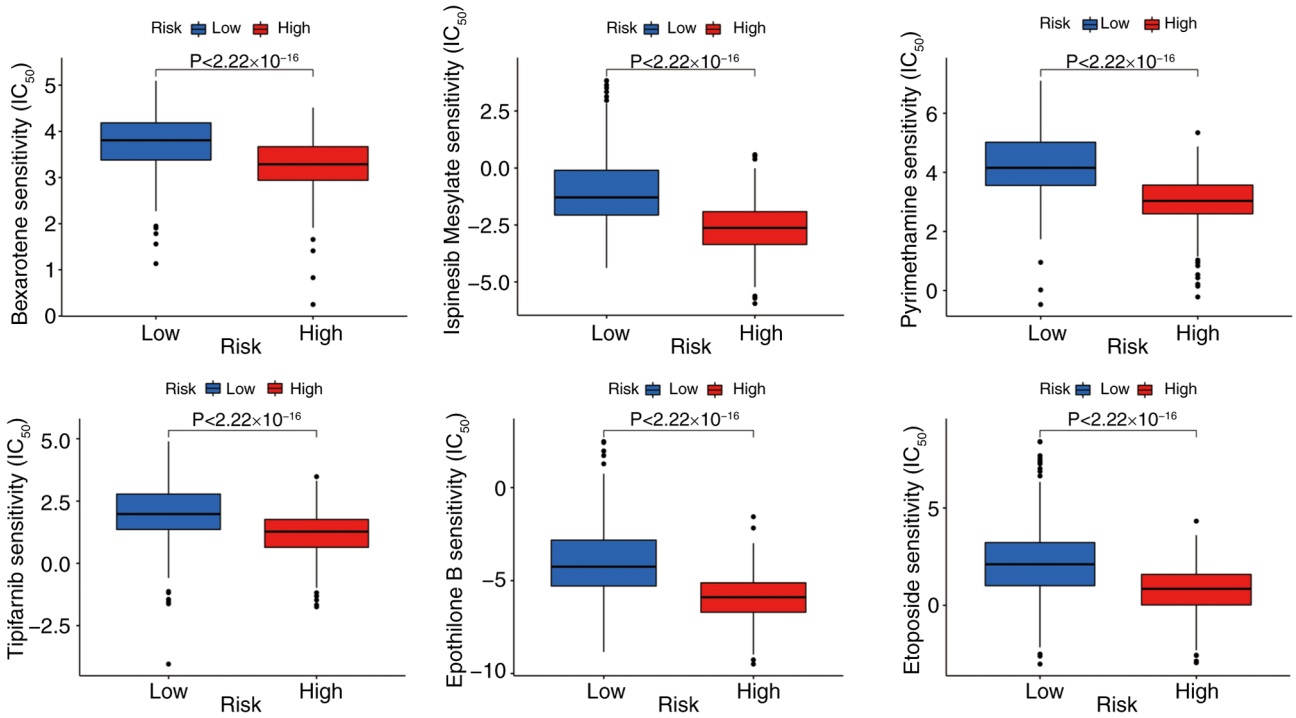

Figure 9. Candidate compounds targeting the four-gene transient receptor potential channel related signature.

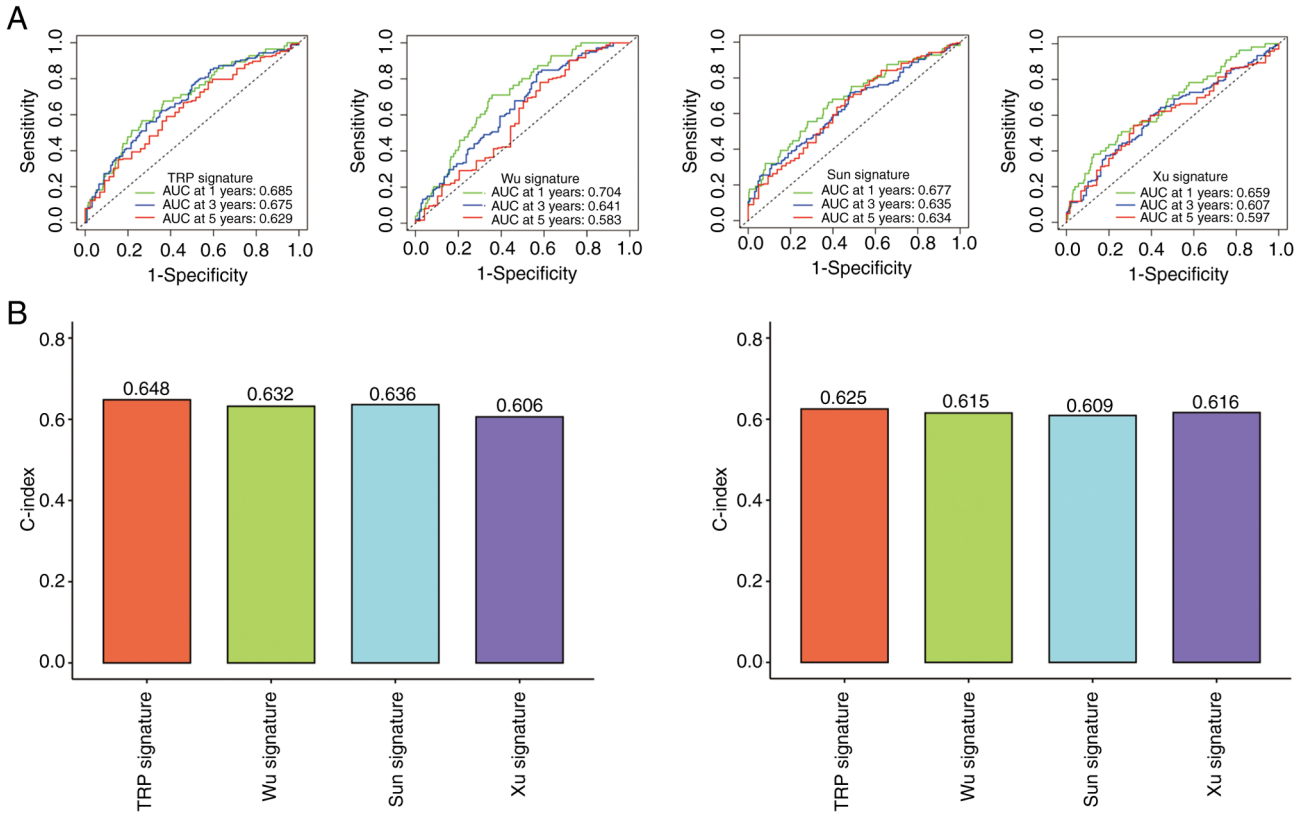

Figure 10. Comparison of the model. Comparison of the prognostic model with previously reported models using (A) receiver operating characteristic curves and (B) C-index values. C-index, concordance index; TRP, transient receptor potential; AUC, area under the curve.

its reliability. Third, while RT-qPCR validation in H1299 cells and cross-dataset consistency (TCGA, Human Protein Atlas and single cell RNA-seq) support the biological plausibility of the signature, the lack of functional evidence in genetically heterogeneous LUAD models warrants investigation. Future work will prioritize mechanistic studies using patient-derived

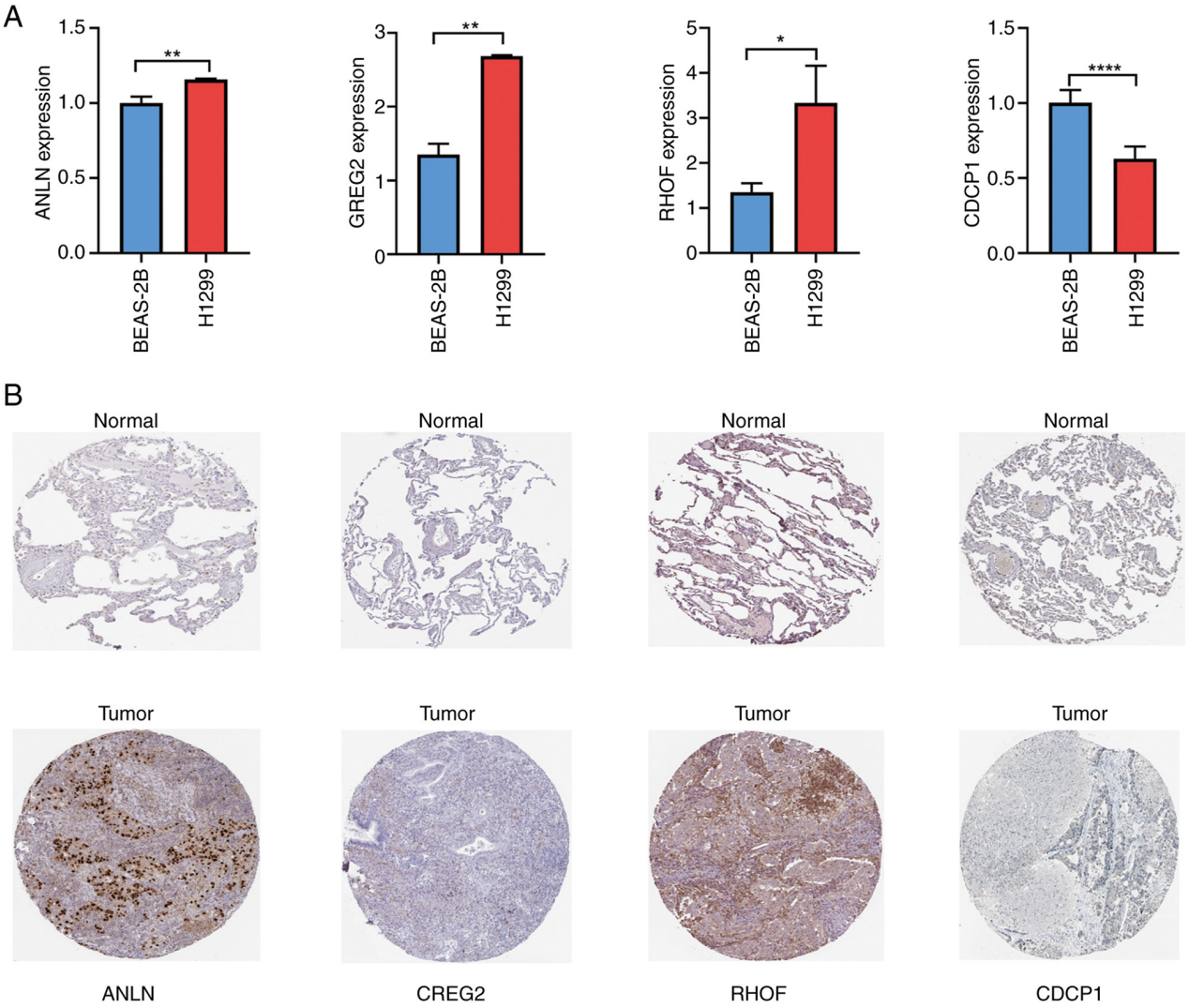

Figure 11. Validation of the four-gene TRP channel related signature expression in LUAD cells. (A) Relative mRNA expression of the genes of the TRP channel related signature in LUAD cell lines. *P<0.05; **P<0.01; ****P<0.0001. (B) Immunohistochemical analysis of the genes of the TRP channel related signature in LUAD tissues from the Human Protein Atlas (www.proteinatlas.org). Data are presented as mean ± SEM. Statistical significance was determined by unpaired two-tailed Student's t-test (n=3 independent experiments). LUAD, lung adenocarcinoma; TRP, transient receptor potential; ANLN, anillin; CREG2, cellular repressor of E1A stimulated genes 2; RHOF, Ras homolog family member F, filopodia associated; CDCP1, CUB domain containing protein 1.

organoids and isogenic cell line panels to address tumor heterogeneity. Fourth, while the prognostic model was validated in both TCGA and GEO cohorts, potential batch effects arising from differences in sequencing platforms, sample collection protocols and normalization methods between these datasets may influence the generalizability of the signature. Fifth, Drug sensitivity (IC_{50}) models rely on cell line data (GDSC), which may not fully reflect *in vivo* tumor complexity; therefore, there is need for clinical validation. Sixth, the lack of validation using tissues from a real-life patient cohort limits the clinical applicability of the present findings. While computational validation through public datasets (TCGA and GEO) provides preliminary support, direct experimental confirmation in prospectively collected clinical specimens is essential to strengthen translational relevance. While the IMvigor210 cohort validates the prognostic utility of the signature in an immunotherapy context, future studies should prioritize LUAD-specific immunotherapy cohorts to confirm translational applicability.

In conclusion, the present study addresses critical gaps in TRP-related LUAD research by delivering a concise, experimentally validated prognostic tool with novel insights into immune modulation and therapeutic response. By focusing on TRP channel-encoding genes, uncovering B-cell interactions and validating immunotherapy utility, the field can be expanded beyond prior metabolic or immune-centric models. These contributions underscore the necessity of the present work and its potential to refine clinical decision-making in LUAD management.

Acknowledgements

Not applicable.

Funding

The present study was supported by '14th Five-Year Plan' Key Discipline-Nantong Medical Innovation Team (Oncology; grant no. 102).

Availability of data and materials

The data generated in the present study may be requested from the corresponding author.

Authors' contributions

DY and SH conceived the project. YC analyzed the data. XF contributed towards the interpretation of the data. All authors wrote, read and approved the final version of the manuscript. DY and SH confirm the authenticity of all the raw data.

Ethics approval and consent to participate

Not applicable.

Patient consent for publication

Not applicable.

Competing interests

The authors declare that they have no competing interests.

References

1. Siegel RL, Kratzer TB, Giaquinto AN, Sung H and Jemal A: Cancer statistics, 2025. CA Cancer J Clin 75: 10-45, 2025.
2. Yang C, Liu Y, Huang Z, Liu S, Zhang X, Liu Q and Dai J: Recent advances and challenges of cellular immunotherapies in lung cancer treatment. Exp Hematol Oncol 14: 94, 2025.
3. No authors listed: Lung Cancer. Am Fam Physician 105: Online, 2022.
4. Zhang Y, Luo G, Etxeberria J and Hao Y: Global patterns and trends in lung cancer incidence: A population-based study. J Thorac Oncol 16: 933-944, 2021.
5. Allemani C, Matsuda T, Di Carlo V, Harewood R, Matz M, Nikšić M, Bonaventure A, Valkov M, Johnson CJ, Estève J, *et al*: Global surveillance of trends in cancer survival 2000-14 (CONCORD-3): Analysis of individual records for 37 513 025 patients diagnosed with one of 18 cancers from 322 population-based registries in 71 countries. Lancet 391: 1023-1075, 2018.
6. Rodrigues T, Sieglitz F and Bernardes GJ: Natural product modulators of transient receptor potential (TRP) channels as potential anti-cancer agents. Chem Soc Rev 45: 6130-6137, 2016.
7. Samanta A, Hughes TET and Moiseenkova-Bell VY: Transient receptor potential (TRP) channels. Subcell Biochem 87: 141-165, 2018.
8. Pan F, Wang K, Zheng M, Ren Y, Hao W and Yan J: A TRP family based signature for prognosis prediction in head and neck squamous cell carcinoma. J Oncol 2022: 8757656, 2022.
9. Ouadid-Ahidouch H, Dhennin-Duthille I, Gautier M, Sevestre H and Ahidouch A: TRP channels: Diagnostic markers and therapeutic targets for breast cancer? Trends Mol Med 19: 117-124, 2013.
10. Büch TRH, Büch EAM, Boekhoff I, Steinritz D and Aigner A: Role of chemosensory TRP channels in lung cancer. Pharmaceuticals (Basel) 11: 90, 2018.
11. Zhao Y, Wang J and Liu X: TRPV4 induces apoptosis via p38 MAPK in human lung cancer cells. Braz J Med Biol Res 54: e10867, 2021.
12. Mounir M, Lucchetta M, Silva TC, Olsen C, Bontempi G, Chen X, Noushmehr H, Colaprico A and Papaleo E: New functionalities in the TCGAbiolinks package for the study and integration of cancer data from GDC and GTEx. PLoS Comput Biol 15: e1006701, 2019.
13. Chen H, Su X, Li Y, Dang C and Luo Z: Identification of metabolic reprogramming-related genes as potential diagnostic biomarkers for diabetic nephropathy based on bioinformatics. Diabetol Metab Syndr 16: 287, 2024.
14. Tu X, Huang H, Xu S, Li C and Luo S: Single-cell transcriptomics reveals immune infiltrate in sepsis. Front Pharmacol 14: 1133145, 2023.
15. Ritchie ME, Phipson B, Wu D, Hu Y, Law CW, Shi W and Smyth GK: limma powers differential expression analyses for RNA-sequencing and microarray studies. Nucleic Acids Res 43: e47, 2015.
16. Wilkerson MD and Hayes DN: ConsensusClusterPlus: A class discovery tool with confidence assessments and item tracking. Bioinformatics 26: 1572-1573, 2010.
17. Tong M, Tu Q, Wang L, Chen H, Wan X and Xu Z: Joint analysis of single-cell RNA sequencing and bulk transcriptome reveals the heterogeneity of the urea cycle of astrocytes in glioblastoma. Neurobiol Dis 208: 106835, 2025.
18. O'Connell TM: Pathway volcano: An interactive tool for pathway guided visualization of differential expression data. Bioinformatics 41: btaf367, 2025.
19. Melit Devassy B, George S and Nussbaum P: Unsupervised clustering of hyperspectral paper data using t-SNE. J Imaging 6: 29, 2020.
20. Zhang S, Huang G, Li X, Zhang Z, Peng K, Zhu L, Zhang C and Niu TT: Global, regional and national retinoblastoma burden in children under 10 years of age from 1990 to 2021: Trend analysis based on the global burden of disease study 2021. PLoS One 20: e0327832, 2025.
21. Li H, Li G, Gao X, Chen C, Cui Z, Cao X and Su J: Development of a reliable risk prognostic model for lung adenocarcinoma based on the genes related to endotheliocyte senescence. Sci Rep 15: 12604, 2025.
22. Chen X, Chen W, Zhou J, Chen J, Cao G, Huang C, Lu X, Chen X, Luo R, Huang H, *et al*: Association between early antibiotic treatment after admission and mortality of acute-on-chronic liver failure patients with bacterial infection: A multicenter retrospective study. Virulence 16: 2509757, 2025.
23. Li-Fei M, Ren SM, Wang J, Zhao WJ, Chen J and Hu WT: Risk scoring model for lung adenocarcinoma based on PD-L1 related signature reveals prognostic predictability and correlation with tumor immune microenvironment genes was constructed. Front Immunol 16: 1601982, 2025.
24. Hänzelmann S, Castelo R and Guinney J: GSVA: Gene set variation analysis for microarray and RNA-seq data. BMC Bioinformatics 14: 7, 2013.
25. SCOT-HEART Investigators; Newby DE, Adamson PD, Berry C, Boon NA, Dweck MR, Flather M, Forbes J, Hunter A, Lewis S, *et al*: Coronary CT angiography and 5-year risk of myocardial infarction. N Engl J Med 379: 924-933, 2018.
26. Livak KJ and Schmittgen TD: Analysis of relative gene expression data using real-time quantitative PCR and the 2(-Delta Delta C(T)) method. Methods 25: 402-408, 2001.
27. Wang N and Liu D: Identification and validation a necroptosis-related prognostic signature and associated regulatory axis in stomach adenocarcinoma. Onco Targets Ther 14: 5373-5383, 2021.
28. Sun S, Wang Y, Li M and Wu J: Identification of TRP-related subtypes, development of a prognostic model, and characterization of tumor microenvironment infiltration in lung adenocarcinoma. Front Mol Biosci 9: 861380, 2022.
29. Wu J, Li L, Zhang H, Zhao Y, Zhang H, Wu S and Xu B: A risk model developed based on tumor microenvironment predicts overall survival and associates with tumor immunity of patients with lung adenocarcinoma. Oncogene 40: 4413-4424, 2021.
30. Xu Q and Chen Y: An aging-related gene signature-based model for risk stratification and prognosis prediction in lung adenocarcinoma. Front Cell Dev Biol 9: 685379, 2021.
31. Suzuki C, Daigo Y, Ishikawa N, Kato T, Hayama S, Ito T, Tsuchiya E and Nakamura Y: ANLN plays a critical role in human lung carcinogenesis through the activation of RHOA and by involvement in the phosphoinositide 3-kinase/AKT pathway. Cancer Res 65: 11314-11325, 2005.
32. Xu J, Zheng H, Yuan S, Zhou B, Zhao W, Pan Y and Qi D: Overexpression of ANLN in lung adenocarcinoma is associated with metastasis. Thorac Cancer 10: 1702-1709, 2019.
33. Li S, Liu Y, Bai Y, Chen M, Cheng D, Wu M and Xia J: Ras homolog family member F, filopodia associated promotes hepatocellular carcinoma metastasis by altering the metabolic status of cancer cells through RAB3D. Hepatology 73: 2361-2379, 2021.
34. Kunita R, Otomo A and Ikeda JE: Identification and characterization of novel members of the CREG family, putative secreted glycoproteins expressed specifically in brain. Genomics 80: 456-460, 2002.

35. Weivoda MM, Chew CK, Monroe DG, Farr JN, Atkinson EJ, Geske JR, Eckhardt B, Thicke B, Ruan M, Tweed AJ, *et al*: Identification of osteoclast-osteoblast coupling factors in humans reveals links between bone and energy metabolism. Nat Commun 11: 87, 2020.
36. He Y, Davies CM, Harrington BS, Hellmers L, Sheng Y, Broomfield A, McGann T, Bastick K, Zhong L, Wu A, *et al*: CDCP1 enhances Wnt signaling in colorectal cancer promoting nuclear localization of β-catenin and E-cadherin. Oncogene 39: 219-233, 2020.
37. Khan T, Kryza T, Lyons NJ, He Y and Hooper JD: The CDCP1 signaling hub: A target for cancer detection and therapeutic intervention. Cancer Res 81: 2259-2269, 2021.
38. Alajati A, D'Ambrosio M, Troiani M, Mosole S, Pellegrini L, Chen J, Revandkar A, Bolis M, Theurillat JP, Guccini I, *et al*: CDCP1 overexpression drives prostate cancer progression and can be targeted in vivo. J Clin Invest 130: 2435-2450, 2020.
39. Hwang SM, Lee JY, Park CK and Kim YH: The role of TRP channels and PMCA in brain disorders: Intracellular calcium and pH homeostasis. Front Cell Dev Biol 9: 584388, 2021.
40. Balood M, Ahmadi M, Eichwald T, Ahmadi A, Majdoubi A, Roversi K, Roversi K, Lucido CT, Restaino AC, Huang S, *et al*: Nociceptor neurons affect cancer immunosurveillance. Nature 611: 405-412, 2022.
41. Lory NC, Nawrocki M, Corazza M, Schmid J, Schumacher V, Bedke T, Menzel S, Koch-Nolte F, Guse AH, Huber S and Mittrücker HW: TRPM2 is not required for T-Cell activation and differentiation. Front Immunol 12: 778916, 2022.
42. Kozai D, Ogawa N and Mori Y: Redox regulation of transient receptor potential channels. Antioxid Redox Signal 21: 971-986, 2014.
43. Sullivan JM, Bagnell AM, Alevy J, Avila EM, Mihaljević L, Saavedra-Rivera PC, Kong L, Huh JS, McCray BA, Aisenberg WH, *et al*: Gain-of-function mutations of TRPV4 acting in endothelial cells drive blood-CNS barrier breakdown and motor neuron degeneration in mice. Sci Transl Med 16: eadk1358, 2024.
44. Tian X, Nanding K, Dai X, Wang Q, Wang J, Morigen and Fan L: Pattern recognition receptor mediated innate immune response requires a Rif-dependent pathway. J Autoimmun 134: 102975, 2023.
45. Liang Q, Wang JW, Bai YR, Li RL, Wu CJ and Peng W: Targeting TRPV1 and TRPA1: A feasible strategy for natural herbal medicines to combat postoperative ileus. Pharmacol Res 196: 106923, 2023.
46. Datta A, Lee JH, Flandrin O, Horneman H, Lee J, Metruccio MME, Bautista D, Evans DJ and Fleiszig SMJ: TRPA1 and TPRV1 ion channels are required for contact lens-induced corneal parainflammation and can modulate levels of resident corneal immune cells. Invest Ophthalmol Vis Sci 64: 21, 2023.
47. He M, Wu G, Wang Z, Ren K, Yang Z and Xue Q: Development and validation of a TRP-related gene signature for overall survival prediction in lung adenocarcinoma. Front Genet 13: 905650, 2022.
48. Wang Z, Zhang J, Zuo C, Chen H, Wang L, Xie Y, Ma H, Min S, Wang X and Lian C: Identification and validation of tryptophan-related gene signatures to predict prognosis and immunotherapy response in lung adenocarcinoma reveals a critical role for PTTG1. Front Immunol 15: 1386427, 2024.
49. Guo Y and Liu N: Systematic analysis and identification of molecular subtypes of TRP-related genes and prognosis prediction in lung adenocarcinoma. J Oncol 2022: 5388283, 2022.